Received: 19 March 2021 | Revised: 16 July 2021 | Accepted: 15 August 2021

DOI: 10.1002/cne.25237

RESEARCH ARTICLE

JCN RESEARCH IN SYSTEMS NEUROSCIENCE THE JOURNAL OF COMPARATIVE NEUROLOGY WILEY

Constitutive tumor necrosis factor (TNF)-deficiency causes a reduction in spine density in mouse dentate granule cells accompanied by homeostatic adaptations of spine head size

Dinko Smilovic[1,2] | Michael Rietsche[1] | Alexander Drakew[1] | Mario Vuksic[1,2] | Thomas Deller[1]

[1] Institute of Clinical Neuroanatomy, Dr. Senckenberg Anatomy, Neuroscience Center, Goethe University Frankfurt, Frankfurt/Main, Germany

[2] Croatian Institute for Brain Research, School of Medicine, University of Zagreb, Zagreb, Croatia

Correspondence
Thomas Deller, Institute of Clinical Neuroanatomy, Dr. Senckenberg Anatomy, Neuroscience Center, Goethe University Frankfurt, Theodor-Stern-Kai 7, Frankfurt/Main, D-60590, Germany.
Email: t.deller@em.uni-frankfurt.de

Funding information
Ministry of Science and Education of the Republic of Croatia and Deutscher Akademischer Austauschdienst (MZOŠ-DAAD), Grant/Award Number: GA KK01.1.1.01.007; Deutsche Forschungsgemeinschaft, Grant/Award Number: CRC1080; European Union, Grant/Award Number: GAKK01.1.1.01.007; European Union, Grant/Award Number: Europass Mobility grant; Dr. Senckenbergische Stiftung

Abstract

The majority of excitatory synapses terminating on cortical neurons are found on dendritic spines. The geometry of spines, in particular the size of the spine head, tightly correlates with the strength of the excitatory synapse formed with the spine. Under conditions of synaptic plasticity, spine geometry may change, reflecting functional adaptations. Since the cytokine tumor necrosis factor (TNF) has been shown to influence synaptic transmission as well as Hebbian and homeostatic forms of synaptic plasticity, we speculated that TNF-deficiency may cause concomitant structural changes at the level of dendritic spines. To address this question, we analyzed spine density and spine head area of Alexa568-filled granule cells in the dentate gyrus of adult C57BL/6J and TNF-deficient (TNF-KO) mice. Tissue sections were double-stained for the actin-modulating and plasticity-related protein synaptopodin (SP), a molecular marker for strong and stable spines. Dendritic segments of TNF-deficient granule cells exhibited ~20% fewer spines in the outer molecular layer of the dentate gyrus compared to controls, indicating a reduced afferent innervation. Of note, these segments also had larger spines containing larger SP-clusters. This pattern of changes is strikingly similar to the one seen after denervation-associated spine loss following experimental entorhinal denervation of granule cells: Denervated granule cells increase the SP-content and strength of their remaining spines to homeostatically compensate for those that were lost. Our data suggest a similar compensatory mechanism in TNF-deficient granule cells in response to a reduction in their afferent innervation.

KEYWORDS
dentate gyrus, homeostatic plasticity, spine head, synaptic plasticity, synaptopodin, tumor necrosis factor

1 | INTRODUCTION

Dendritic spines are highly motile protrusions on dendrites of many neurons in the central nervous system (Dunaevsky et al., 2001) forming axo-spinous synapses with glutamatergic afferents (DeFelipe et al., 1988). They are basic functional units of signal integration detecting the coincidence of pre- and postsynaptic activity (Yuste & Denk, 1995). Of note, spines are modified by synaptic activity and the geometry of spines has been tightly linked to the functional properties of their synapses (Bonhoeffer & Yuste, 2002; Kasai et al., 2003; Matsuzaki et al., 2004). In particular, spine head size is associated with synaptic strength (Fifková & van Harreveld, 1977; Kasai et al., 2010; McKinney, 2010), postsynaptic density area (Harris et al., 1992), and AMPA-receptor density (Matsuzaki et al., 2001, 2004; Noguchi et al., 2011; Zito et al., 2009), thus making spine head size a structural surrogate marker – or at least an indicator – for local synaptic activity.

Tumor necrosis factor (TNF) is a pleiotropic cytokine that has been implicated in a wide range of physiological, that is, synaptic plasticity (Heir & Stellwagen, 2020; Santello & Volterra, 2012) and pathophysiological processes, that is, inflammation (Locksley et al., 2001; Santello & Volterra, 2012). In the central nervous system, TNF has also been shown to affect synaptic function with its net effect depending strongly on its concentration (Heir & Stellwagen, 2020; Maggio & Vlachos, 2018; Santello & Volterra, 2012). At low concentrations, that is, in a physiologic range, TNF increases synaptic strength (Stellwagen & Malenka, 2006; Stellwagen et al., 2005). It is also permissive for different forms of homeostatic synaptic plasticity (Becker et al., 2013; Steinmetz & Turrigiano, 2010; Stellwagen & Malenka, 2006) and it has recently been shown to promote the ability of neurons to express LTP (long-term potentiation; Maggio & Vlachos, 2018). Since TNF also reduces GABAergic transmission by promoting GABAa-receptor endocytosis (Stellwagen et al., 2005), TNF has been suggested to play a role in the fine tuning of excitation/inhibition of neuronal networks (Santello & Volterra, 2012; Stellwagen et al., 2005). These physiological functions of TNF, which require only basal concentrations of the cytokine are considered largely distinct from TNF actions in pathophysiological contexts (Heir & Stellwagen, 2020; Santello & Volterra, 2012).

Synaptopodin (SP) is an actin-modulating protein expressed in kidney podocytes and telencephalic neurons (Mundel et al., 1997). In spine-bearing neurons it is found in ~10-15% of spines, in particular in the functionally important subgroup of large and stable spines (Yap et al., 2020). SP is required for the formation of a spine apparatus organelle, that is, an internal calcium store consisting of stacks of endoplasmic reticulum and dense plates (Deller et al., 2000, 2003; Gray, 1959; Spacek, 1985). The spine apparatus promotes AMPA-R accumulation at excitatory synapses and SP/spine apparatus are part of the downstream machinery changing synaptic strength (Jedlicka & Deller, 2017; Korkotian et al., 2014; Vlachos et al., 2009). Accordingly, mice lacking SP show deficits in Hebbian (Deller et al., 2003; Grigoryan & Segal, 2016; Jedlicka et al., 2009; Jedlicka & Deller, 2017; Vlachos et al., 2009; Zhang et al., 2013), homeostatic (Vlachos, Ikenberg, et al., 2013), and metaplastic (Maggio & Vlachos, 2018) forms of synaptic plasticity. Recently, it has been shown that TNF requires SP for its effects on Hebbian plasticity (Maggio & Vlachos, 2018), suggesting a link between TNF and SP.

Since the number and geometry of spines are tightly linked to synaptic function, and since TNF has been linked to synaptic plasticity and SP, we wondered whether lack of TNF could result in changes of spines and/or SP within spines, which would be indicative of an altered network function. Our data show that constitutive TNF-deficiency does indeed cause structural changes of dendrites of dentate granule cells and suggest that these structural changes reflect a compensatory homeostatic response: TNF-deficient granule cells may compensate a reduced number of dendritic spines, that is, fewer afferent synapses, by homeostatically increasing the strength of some of their remaining spines, that is remaining synapses.

2 | MATERIALS AND METHODS

2.1 | Animals

Adult male mice (10–26 weeks) lacking TNF (TNF-KO, C57BL/6J Jackson Laboratory, Bar Harbor, Maine, RRID: IMSR_JAX:003008; $n = 7$) and their wildtype controls (TNF-WT, C57BL/6J background; $n = 7$) were obtained from heterozygous breeders (TNF±). Mice were bred and housed at the animal facility of the Goethe-University Hospital Frankfurt or at MfD Diagnostics GmbH, Wendelsheim, and were maintained on a 12-h light/dark cycle with food and water available ad libitum. Genotyping was performed at ~3–4 weeks of age. The age distribution of mice in both groups was comparable (Figure 1, Brunner–Munzel *U*-test; n.s. $p = 0.145$). Animals were killed in accordance with the German animal welfare law and had been declared to the Animal Welfare Officer of the Faculty (Wa-2014-35). Every effort was made to minimize distress and pain of animals.

2.2 | Intracellular injections of granule cells in fixed tissue

After delivery, animals were kept in an in-house scantainer for a minimum of 24 h. Animals were killed with an overdose of intraperitoneal pentobarbital and subsequently intracardially perfused (0.1 M Phosphate buffer saline (PBS) containing 4% paraformaldehyde (PFA)). Tail biopsies were obtained after death to reconfirm the genotype. Brains were taken out immediately after perfusion, postfixed (18 h, 4% PFA in 0.1 M PBS, 4°C), washed trice in ice-cold 0.1 M PBS, sectioned (250 μm) on a vibratome (Leica VT 1000 S), and stored at 4°C until use. Intracellular injections of granule cells in fixed slices were performed as previously described (Arends & Jacquin, 1993; Hick et al., 2015; Yap et al., 2020), with modifications. Hippocampal slices were placed in a custom-built, transparent, and grounded recording chamber filled with ice-cold 0.1 M PBS. The chamber was attached to an epifluorescence microscope (Olympus BX51WI; 10× objective LMPlanFLN10×, NA 0.25, WD 21 mm) mounted on an *x-y* translation table (Science Products, VT-1 xy Microscope Translator). Sharp quartz-glass microelectrodes (Sutter Instruments, QF100-70-10, with filament) were pulled

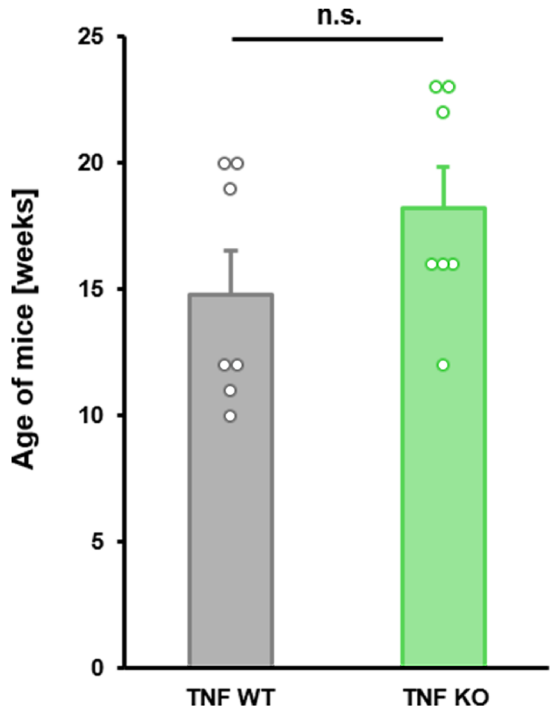

FIGURE 1 Age distribution of TNF-WT and TNF-KO mice. Mice used in the present study were age-matched. There were no significant differences between the age distribution of the two groups. n.s. $p = 0.144$. Brunner–Munzel *U*-test. TNF-WT, $n = 7$; TNF-KO, $n = 7$

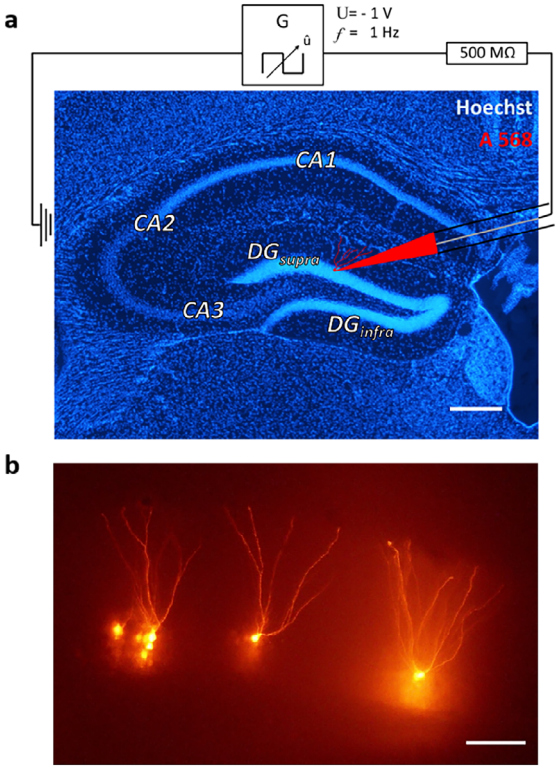

FIGURE 2 Intracellular injections of granule cells in fixed slices. (a) Schematic showing intracellular filling of dentate granule cells in a frontal 250 μm-section of a mouse hippocampus. A quartz electrode loaded with 1 mM Alexa568 dye and backfilled with 0.1 M $LiCl_2$ is used to impale and subsequently fill (10 min) neurons. DG_{supra}: suprapyramidal blade of dentate gyrus. DG_{infra}: infrapyramidal blade of dentate gyrus. CA1, CA2, CA3: Areas 1, 2 and 3 of cornu ammonis. Scale bar = 500 μm. (b) Overview image showing several dye-injected granule cells in the DG_{supra}. Scale bar = 100 μm

using a P-2000 laser puller (Sutter Instruments). Microelectrodes were tip-loaded with 0.75 mM Alexa568-Hydrazide (Invitrogen) in HPLC-grade water (VWR Chemicals, HiPerSolv CHROMANORM) and subsequently back-filled with 0.1 M LiCl in HPLC-grade water. Microelectrodes were attached to an electrophoretic setup via a silver wire and 500 MΩ resistance. The tip of the microelectrode was navigated into the granule cell layer using a micromanipulator (Märzhäuser Wetzlar, Manipulator DC-3K). A square-wave voltage (1 mV, 1 Hz) was applied using a voltage generator (Gwinstek SFG-2102). Granule cells were filled under visual control for at least 10 min or until no further labeling was observed. (Figures 2a and 2b). Injected sections were fixed overnight (4% PFA in PBS, 4°C, in darkness) and washed in 0.1 M PBS.

2.3 | Immunohistochemistry

Filled and fixed injected sections (250 μm) were embedded in 5% agar and resliced into 40 μm thick sections on a vibratome (Leica VT 1000 S). Free-floating sections were washed several times in 50 mM Tris-buffered saline (TBS) containing 0.1% Triton X-100, incubated in a blocking buffer (0.5% Triton X-100, 5% bovine serum albumin (BSA) in 50 mM TBS) for 30 min at room temperature (RT) and subsequently incubated with guinea pig anti-SP (Synaptic Systems, RRID: AB_10549419; 1 mg/ml, 1:2000, diluted in 0.1% Triton X-100, 1%BSA in 50 mM TBS) for 3 days at RT (Paul et al., 2020). The polyclonal SP antibody recognizes AA 331 to 452 of the mouse SP protein (https://sysy.com/product-factsheet/SySy_163004). After several washing steps, sections were incubated with donkey anti guinea pig Alexa Fluor 488 (Jackson ImmunoResearch Labs, RRID: AB_2340472; 1 mg/ml, 1:2000) for 4 h at RT and mounted on slides (Dako fluorescence mounting medium, Dako North America Inc.).

2.4 | Confocal microscopy of fixed hippocampal slices

Confocal imaging of fixed dendritic segments from identified, Alexa568-labeled dentate granule cells in the outer molecular layer (OML) of the suprapyramidal blade was done with an Olympus FV1000 microscope and a 60× oil-immersion objective (UPlanSApo, NA 1.35, Olympus) using FV10-ASW software with 5× scan zoom at a resolution of 1024 × 1024 pixels. To ensure localization of dendritic segments in the OML the hippocampal fissure was used for orientation. Dendritic segments located at a distance of 10–20 μm from the hippocampal fissure were identified and traced for a maximal length of 50 μm. Only segments within the OML were used for analysis and only one dendritic segment was used per labeled cell. Three-dimensional image stacks of such dendritic segments (0.15 μm *z*-axis step size) were

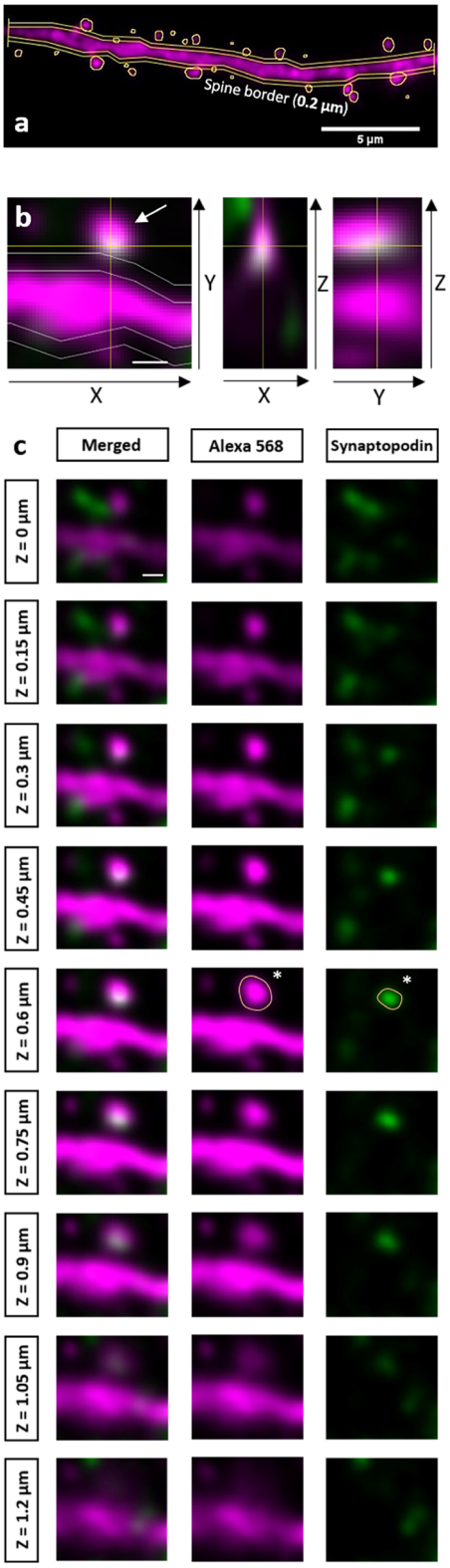

FIGURE 3 Quantification of dendritic spine head area and synaptopodin (SP) cluster area. (a) Maximum projection of a confocal image stack showing a dendritic segment of a granule cell. For analysis, dendritic spines of all shapes were assessed manually on *z*-stacks of dendritic segments. Only protrusions extending laterally in the *x*-*y* plane, not above or below the dendrite, and exceeding the dendrite for at least 5 pixels (0.2 μm) were included for analysis. For spine head area the maximum cross-sectional area of the spine head was identified in one of the *x*-*y* planes and measured. Scale bar = 5 μm. (b) Only spines with heads protruding at least 0.2 μm from the parent dendrite (parallel white lines) were analyzed. Spines co-localizing with an SP cluster in the *x*-*y*, *x*-*z*, and *y*-*z* directions when scrolling through the *z*-stack were considered to be SP+ (arrow). Scale bar = 0.5 μm. (c) Spine head area and SP cluster area were defined as the largest *x*-*y* cross-sectional area obtained in a *z*-stack. Images containing the largest area of spine head (middle column, orange outline of spine head, asterisk) and SP cluster (right column, orange outline of SP-cluster, asterisk) are highlighted. Scale bar = 0.5 μm

acquired. Crossing dendritic segments or branch points were avoided to facilitate spine attribution to a given segment. For imaging of dendritic segments, imaging parameters were set to capture the dendritic segment as bright as possible without oversaturating the spines. For imaging of SP, all imaging parameters were kept the same for all images.

2.5 | Image processing and data analysis

Images obtained were deconvolved with Huygens Professional Version 17.10 (Scientific Volume Imaging, The Netherlands, http://svi.nl). Image processing and data analysis were then performed using Fiji version 1.52h (Schindelin et al., 2012). Spines were identified and analyzed using established criteria (Holtmaat et al., 2009). Prior to quantification, all images were randomized. Images were renamed by one experimenter (M. Rietsche) and subsequently analyzed by a second experimenter (D. Smilovic) blind to genotypes. Dendritic spines of all shapes were assessed manually on *z*-stacks of dendritic segments in the OML. Only protrusions emanating laterally in the *x*-*y* directions, not above or below the dendrite, and exceeding the dendrite for at least 5 pixels (0.2 μm) were included for analysis (Holtmaat et al., 2009; Vlachos, Müller-Dahlhaus, et al., 2012; Yap et al., 2020). The length of each segment was determined (Figure 3a). For spine head area and SP cluster area measurements, the largest maximum cross-sectional area of the spine head or SP cluster in one of the *x*-*y* planes within the *z*-stack was manually measured using a predefined gray-value as a cutoff for the border of the spine head or SP cluster (Figure 3b). A spine was considered SP+ if the SP cluster overlapped with the spine head, neck, and/or base in both the *x*-*z* and *y*-*z* directions when scrolling through the *z*-stacks (Figure 3c). The subcellular location of SP clusters in the spine head, spine neck, spine base, or dendritic segment was noted. SP clusters were considered within the spine head, if most (> 80%) of the SP-cluster was located within the identified area of the spine head (see Figure 3c). SP-clusters were considered within the spine neck, if most (> 80%) of the cluster was located outside the dendritic shaft border, between the identified area of the spine head and the shaft, where a fluorescently filled, visible, spine neck was marked. SP clusters were considered associated with the spine base, if they were found within 0.2 μm of the intersection between the dendritic spine and the dendritic shaft border. SP clusters were considered inside dendritic shafts if they did not meet any of the aforementioned criteria but were still localized within the investigated dendritic segment.

2.6 | Statistical analysis

Statistical tests and *n*-values used for testing are indicated in the figure captions. Statistical analysis was performed using R 4.0.4 (R Core Team, 2013) called via R-script from LabVIEW scripts (National Instruments, Austin, Texas). Robust methods were applied throughout as specified for the different conditions: (1) Comparison of magnitude between two groups: Brunner–Munzel *U*-test (function "brunnermunzel.permutation.test" from R-library "brunnermunzel") (Brunner & Munzel, 2000), (2) comparison of two distributions: Cramer-von Mises test ("cvm_test" from R-library "twosamples"), (3) comparison of proportions of occurrences between two groups: Log-likelihood ratio test (*G*-test) of independence ("GTest" from R-library "DescTools"). In case of 2 × 3 tables, post hoc *G*-tests were applied on item versus sum of the other items, (4) comparison of proportions of occurrences against a given set of proportions: *G*-test as goodness-of-fit test ("GTest" with given proportions) , (5) comparisons of means between groups owning levels of two crossed factors (TNF genotype and SP content of spines): robust multivariate analysis of variance (MANOVA (Friedrich et al., 2019)), and univariate (post hoc) tests (function "MANOVA.wide" from R-library "MANOVA.RM, considering the test statistic MATS employing parametric bootstrap resampling), (6) measure of association between two attributes: Spearman's rho (R-function "cor" employing method "spearman"), and (7) robust linear regression between two attributes: R-function "rlm" employing method "MM" from library "MASS". Confidence intervals for Spearman's rho and for regression slope and intercept were obtained using the resampling function "bootstrap" from R-library "bootstrap." In case of multiple post hoc tests *p*-values were adjusted using the function "p.adjust" employing method "hochberg". If *p* values were less than 0.05, the null-hypothesis was rejected ($^{*}p < 0.05$, $^{**}p < 0.01$, $^{***}p < 0.001$). Quantitative data are displayed either in box plots (box encloses 25-75% quartiles, dividing line in box represents median, x labels mean, whiskers represent maximum / minimum or median ± 1.5 times the distance between the 25% and 75% quartiles in case of presence of extreme values, which are shown as additional dots) or as bar plots (mean + *SEM*) including the individual data points as dots. Diagrams were created using Microsoft Office Excel.

3 | RESULTS

3.1 | Granule cell dendrites of TNF-KO mice exhibit a reduced spine density

Previous work showed that TNF is an important factor in the control of synaptic strength (Beattie et al., 2002; Santello et al., 2011; Stellwagen et al., 2005; Stück et al., 2012). Since synaptic strength and spine geometry are tightly linked (Bonhoeffer & Yuste, 2002; Fifková & van Harreveld, 1977; Kasai et al., 2003; Matsuzaki et al., 2004), we speculated that genetic knockout of TNF in vivo may have a structural correlate at the level of spines. To address this question, we first studied dendritic segments of Alexa568-filled granule cells (Figure 4a–c) in the outer molecular layer of the DG of TNF-deficient and age-matched C57BL/6J control mice. TNF-KO mice exhibited a significant reduction in spine density (Figure 4d): whereas wildtype mice had 2.03 spines/μm, TNF-KO mice had 1.62 spines/μm, that is, ~20% fewer spines. Next, we analyzed spine head area, since spine head area correlates well with synaptic strength and the density of AMPA-Rs. Average spine head area was not significantly different between genotypes (Figure 4e), although a trend towards higher values was seen in TNF-KO segments. Finally, we calculated total spine head area per segment (Figure 4f), which illustrates how changes in spine density and head area affect the available spine head area for neurotransmission. This parameter takes the number of spines into account and shows that the total spine head area per segment decreases in the TNF-KO mice. After analyzing dendritic segments, we shifted our attention to the entire population of spines. The trend seen in Figure 4e was confirmed to be significant (Figure 4g). The cumulative distribution revealed a highly significant difference between the two genotypes, with differences most prominent at the beginning of the curve, that is, small spine heads, and at the end of the curve, that is, large spine heads (Figure 4h).

3.2 | TNF-KO mice show an increase in the fraction and size of large spines

To investigate this further, we distinguished three categories of spines (Figure 5a): small (< 0.15 μm^2), medium (0.15 – 0.30 μm^2), and large (> 0.30 μm^2) sized spines and compared average spine head area between control and TNF-KO spines. Although average spine head areas were not different for medium sized spines, large spines were ~19% bigger and small spines were ~8% smaller in TNF-deficient granule cells (Figure 5b). These changes in spine head areas were mirrored by a significant shift in the proportions of fractions of spines belonging to each of the three categories (Figure 5c): TNF-deficient granule cells mice had more small (~54% compared to ~49%) and large (~17% compared to ~13%) sized spines than controls, whereas TNF-WT granule cells had more medium sized spines (~38% compared to ~30%) compared to TNF-deficient cells.

3.3 | SP-positive spines are larger in TNF-KO mice compared to wildtype

Because of the conspicuous increase in the head area of large spines, we wondered about the distribution of the actin-modulating and plasticity-related protein SP, which is primarily associated with this subgroup of spines (Deller et al., 2003; Lenz et al., 2021; Vlachos, Ikenberg, et al., 2013; Yap et al., 2020). Using a double-labeling approach, Alexa568-injected granule cells were also immunolabeled for SP (Figures 6a and 6b). As previously described, SP clusters were abundant in the molecular layer of the DG (Bas Orth et al., 2005; Deller et al., 2000). Using single identified granule cell segments, the presence or absence of SP within spines was noted and the maximum spine head area as well as the maximum cross-sectional area of SP clusters were measured (Figure 3). In both genotypes, the majority of spines were

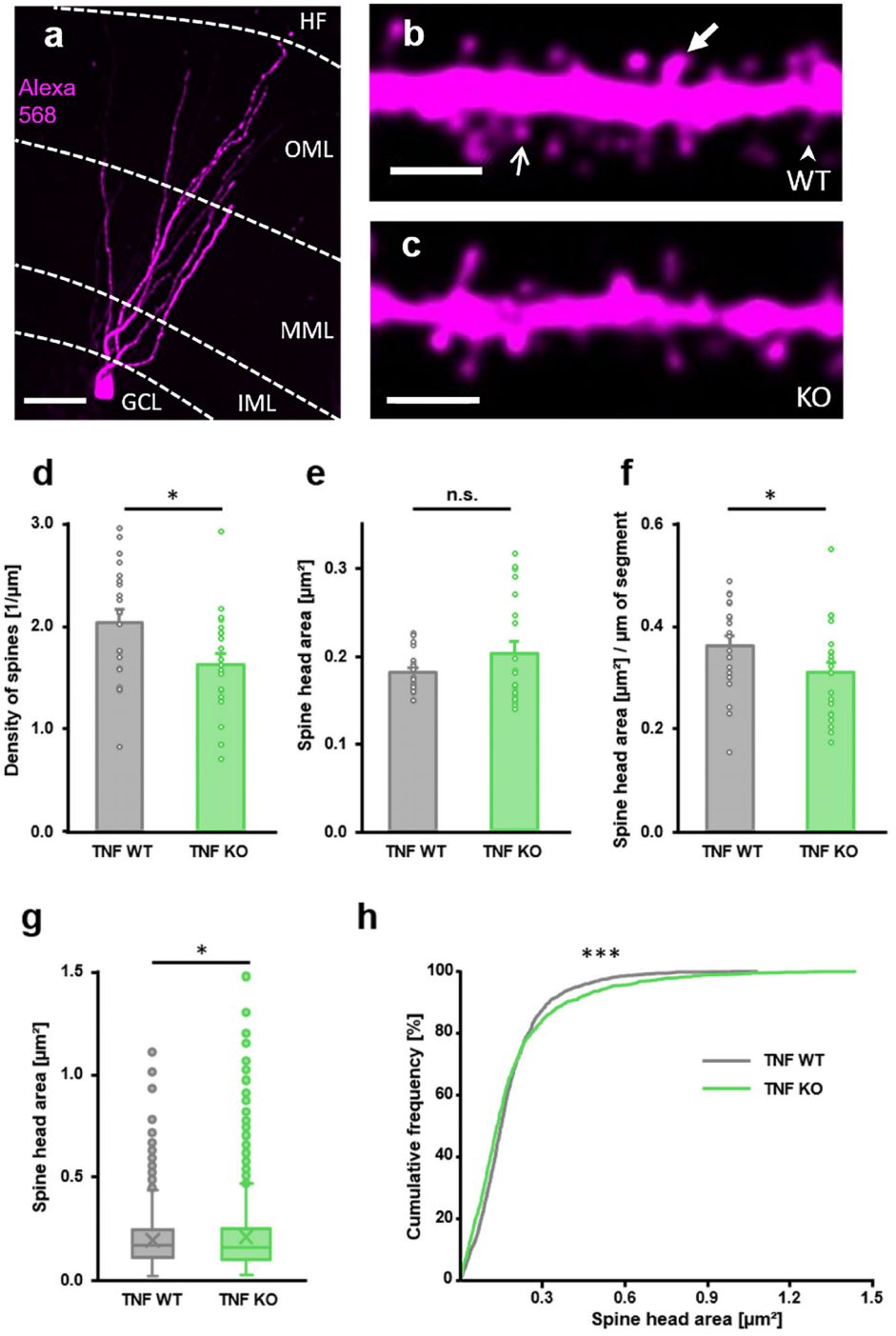

FIGURE 4 Granule cell dendrites of TNF-KO mice exhibit a reduced spine density. (a) Granule cell in the suprapyramidal blade of the dentate gyrus of a TNF-alpha-knock-out (TNF-KO) mouse intracellularly filled with the fluorescent dye Alexa568 hydrazide (magenta; fixed tissue). Dendritic segments in the outer molecular layer (OML) were used for analysis. MML: middle molecular layer. IML: inner molecular layer. GCL: granule cell layer. HF: hippocampal fissure. Scale bar = 20 μm. (b, c) Single confocal sections of granule cell dendrites in the OML of TNF-WT (b) and TNF-KO (c) mice. Scale bar = 2 μm. Large (thick arrow), medium (thin arrow), and small (arrowhead) spines are indicated. (d) Density of dendritic spines on TNF-KO segments is significantly reduced (~1.62 1/μm) compared to controls (~2.03 1/μm). Analysis based on 7 WT and 7 KO mice; 1 segment per cell; 3 dendritic segments per animal (n = 21 segments); 1632 TNF-WT; 1303 TNF-KO spines. *p = 0.0123, Brunner–Munzel U-test. (e) Average spine head area per segment of TNF-WT (~0.18 μm^2) and TNF-KO (~0.20 μm^2) mice are not significantly (n.s.) different; p = 0.991; Brunner–Munzel U-test; n = 21 segments per group. (f) Total spine head area of all spines of a segment divided by the length of the analyzed segment shows a ~14% reduction in spine head area per μm of the segment for TNF-KO (~0.31 μm^2/μm) compared to TNF-WT (~0.36 μm^2/μm), *p = 0.0385; Brunner–Munzel U-test. n = 21 segments per group. (g) Box plots of spine head area of all spines from all segments. Spine heads of TNF-KO mice (0.190 μm^2) are larger than spine heads of TNF-WT mice (0.178 μm^2); 1632 TNF-WT; 1303 TNF-KO spines. *p = 0.0311, Brunner–Munzel U-test. (h) Cumulative frequency plot of these spine head areas. Distributions are different between genotypes; ***p < 0.001; Cramer–von Mises test

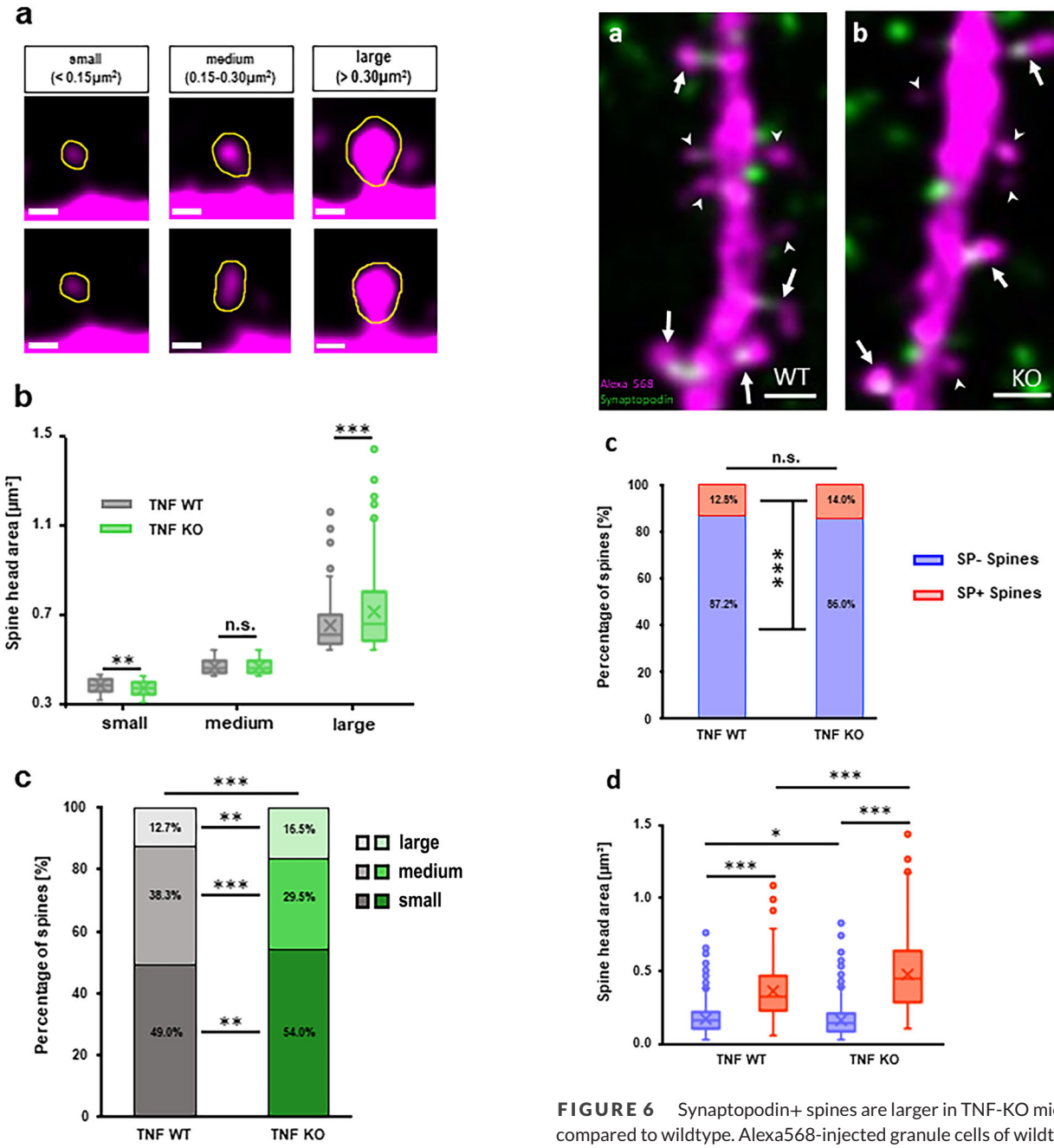

FIGURE 5 TNF-KO mice show an increase in the fraction and area of large spines. (a) Spines were divided into three classes: small (<0.15 μm^2), medium (0.15–0.30 μm^2), and large (>0.30 μm^2) spines. Scale bar = 0.5 μm. (b) Box plots of spine head area of all spines from all segments allocated to the three size classes. Large spines were ~19% bigger in TNF-KO mice (~0.52 μm^2) compared to TNF-WT mice (~0.43 μm^2); ***$p < 0.001$; while small sized TNF-KO spines (~0.0815 μm^2) were ~8% smaller compared to TNF-WT spines (~0.0885 μm^2); **$p = 0.001$. Medium sized spines were not significantly (n.s.) different. $p = 0.637$; univariate robust MANOVA separately for the three size classes; TNF-WT $n = 800, 625, 207$; TNF-KO $n = 703; 385; 215$ (small/medium/large). (c) Proportions of spine numbers allocated to the three size classes were different between genotypes; ***$p < 0.001$; *G*-test of independence. TNF-KO mice had more large (~17% compared to ~13%; **$p = 0.008$; post hoc *G*-test) and more small (~54% compared to ~49%; **$p = 0.007$; post hoc *G*-test) spines and fewer medium spines (~30% compared to ~38%; ***$p < 0.001$; post hoc *G*-test) compared to WT

FIGURE 6 Synaptopodin+ spines are larger in TNF-KO mice compared to wildtype. Alexa568-injected granule cells of wildtype (a) and TNF-KO (b) mice were double-labeled for Synaptopodin (SP; green). Arrows point to SP-positive (SP+) spines; Arrowheads mark SP-negative (SP−) spines. Scale bars = 1 μm. (c) Proportions of fractions of SP+ and SP− spines are not different between genotypes; n.s. $p = 0.328$; *G*-test of independence. Proportion of fractions of SP− in TNF-WT ($n = 1423$, ~87.2%) and in TNF-KO ($n = 1120$, ~86.0%) and fractions of SP+ ($n = 209$, ~12.8%) spines in TNF-WT and SP+ ($n = 183$, ~14.0%) spines in TNF-KO animals differed from equality (50% for SP+ and SP−, respectively); ***$p < 0.001$, *G*-test of goodness of fit. (d) Box plots of head area of SP+ and SP− spines of TNF-WT and TNF-KO animals. (TNF-WT ~0.35 μm^2 SP+ ($n = 209$); ~0.15 μm^2 SP− ($n = 1423$); TNF-KO ~0.45 μm^2 SP+ ($n = 183$), ~0.15 μm^2 SP−($n = 1120$)). SP+ spines have larger spine head areas compared to SP− spines in both genotypes. ***$p < 0.001$; univariate post hoc tests following robust MANOVA. SP+ spines were larger in TNF-KO mice (***$p < 0.001$), whereas SP− spines were smaller in TNF-KO mice, *$p = 0.04$; univariate post-hoc tests following robust MANOVA with *p*-values adjusted for multiple comparisons

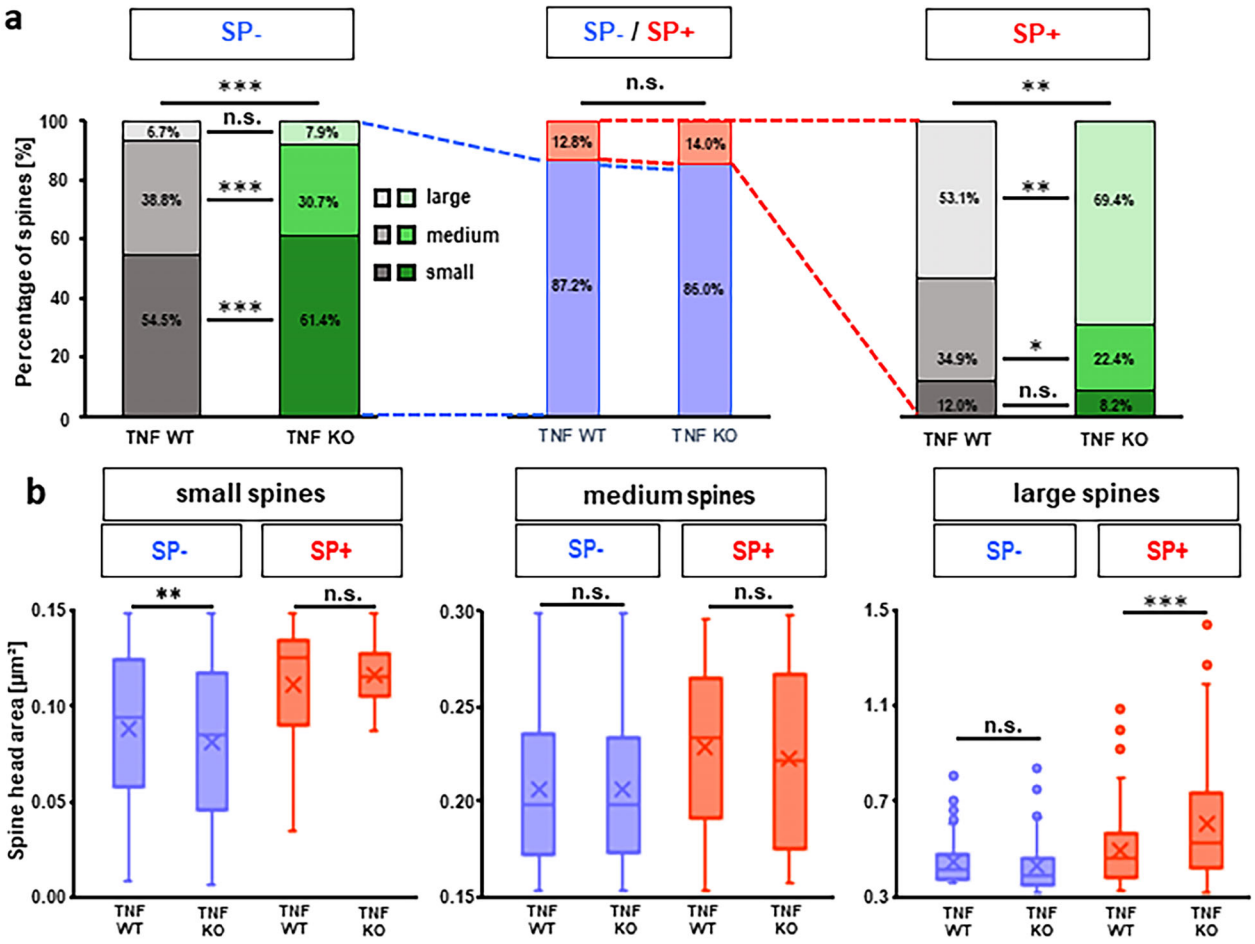

FIGURE 7 Large SP+ spines are selectively enlarged in TNF-KO mice. (a) Proportions of fractions of spines allocated to the three size classes separately for SP− (left panel, blue in the middle panel) and SP+ (right hand panel, red in the middle panel) spines. For both, SP− and SP+ spines, the proportions were different between TNF-WT and TNF-KO mice; $^{***}p < 0.001$ for SP− and $^{**}p = 0.004$ for SP+; *G*-test of independence. In both genotypes, the majority of SP− spines were small spines and the majority of SP+ spines were large spines. Of note, the fraction of large SP+ spines ($^{**}p = 0.003$; post hoc *G*-test) as well as the fraction of small SP− spines ($^{***}p < 0.001$; post hoc *G*-test) were larger in TNF-KO mice, whereas the fraction of medium SP− spines ($^{***}p < 0.001$; post hoc *G*-test) as well as medium SP+ spines ($^{*}p = 0.0123$; post hoc *G*-test) was smaller in TNF-KO mice. Fractions of large SP− ($p = 0.284$; post hoc *G*-test) as well as small SP+ spines ($p = 0.216$; post hoc *G*-test) did not differ significantly between genotypes. Numbers of occurences: TNF-WT: SP− spines $n = 1423$ total; $n = 775/552/96$ small/medium/large SP− spines; SP+ spines $n = 209$ total; $n = 25/73/111$ small/medium/large SP+ spines; TNF-KO: SP− spines $n = 1120$ total; 688/344/88 small/medium/large SP− spines; SP+ spines $n = 183$ total; $n =$ 15/41/127 small/medium/large SP+ spines. (b) Box plots of head area of SP+ and SP− spines of TNF-WT and TNF-KO animals separately for the three size classes. TNF-KO mice have bigger large sized SP+ spines (~0.58 μm^2) compared to WT (~0.46 μm^2) ($^{***}p < 0.001$) and smaller small sized SP− spines (~0.08 μm^2) compared to WT (~0.09 μm^2) ($^{**}p = 0.003$). Differences between other groups were not significant (n.s.): Small SP+ spines (WT: ~0.111 μm^2, KO: ~0.116 μm^2. $p = 0.593$); medium SP− (WT: ~0.205 μm^2, KO: ~0.205 μm^2. $p = 0.862$); medium SP+ (WT: ~0.227 μm^2, KO: ~0.221 μm^2. $p = 0.862$); large SP− (WT: ~0.386 μm^2, KO: 0.413 μm^2. $p = 0.092$); post hoc univariate pairwise comparisons following robust MANOVA with *p*-values adjusted for multiple comparisons

SP− (TNF-WT, 12.8% SP+; 87.2% SP−; TNF-KO, 14.0% SP+; 86.0% SP−; Figure 6c; $^{***}p < 0.001$) and SP+ spines were significantly larger than SP− spines in both genotypes (Figure 6d; $^{***}p < 0.001$). We also noticed that SP+ spines were larger in TNF-KO mice (Figure 6d; $^{***}p < 0.001$) whereas SP− spines were smaller (Figure 6d; $^{*}p = 0.04$) (TNF-WT ~0.35 μm^2 SP+; ~0.15 μm^2 SP−; TNF-KO ~0.45 μm^2 SP+, ~0.15 μm^2 SP−). Since the overall density of spines is lower in TNF-deficient granule cells (Figure 4) and the fraction of SP+ spines is constant, the absolute number of SP+ spines is, however, reduced by ~14% in the TNF-KO.

3.4 | Large SP ± spines are selectively enlarged in TNF-KO mice

We now divided SP+ and SP− spines into the three size categories (c.f. Figures 5a and 5b). Most SP+ spines were found belonging to the large spine category (TNF-WT ~53.1%, TNF-KO ~69.4%; Figure 7a), whereas only few SP− spines were in this category (TNF-WT ~6.7%; TNF-KO ~7.9%, Figure 7a). In the subgroup of large spines, SP+ spines were ~23% bigger in TNF-KO mice compared to controls (Figure 7b; $^{***}p < 0.001$) whereas large SP− spines were not different

between genotypes (Figure 7b; n.s. $p = 0.092$). In the subgroup of small spines, SP+ spines were rare (TNF-WT ~12.0%, TNF-KO ~8.2%; Figure 7a), whereas SP− spines were abundant (TNF-WT ~54.5%, TNF-KO ~61.4%; Figure 7a). SP+ spines belonging to the small category did not differ significantly between TNF-deficient and TNF-WT granule cells (Figure 7b; n.s. $p = 0.593$). In contrast, SP− spines showed a significant reduction of ~10% in spine head area in TNF-KO mice (Figure 7b; $^{**}p = 0.003$). There was no significant difference between genotypes for spines belonging to the medium sized subgroup (n.s. $p = 0.862$ for both, SP+ and SP− spines; Figure 7b). We conclude from these findings, that (i) the increase in spine head area of large spines observed in TNF-KO granule cells (Figure 5b) is the result of an enlargement of large SP+ spines (Figure 7b), and, (ii) the reduction in spine head area of small spines (Figure 5b) is the result of a diminution of small SP− spines (Figure 7b).

3.5 | SP cluster size is increased in spines of TNF-deficient granule cells

The fact that SP+ spines of TNF-deficient granule cells have larger heads made us wonder whether this increase is matched by a corresponding increase in SP clusters, since these two parameters are highly correlated (Lenz et al., 2021; Yap et al., 2020). Indeed, average SP cluster areas were ~25% bigger in TNF-deficient granule cell segments (Figure 8a). Similarly, the cumulative distribution of SP cluster areas was right-shifted in the mouse mutant compared to control (Figure 8b). SP-clusters were preferentially found in the spine head of both genotypes, without a significant shift in proportions between genotypes (Figure 8c, d). Finally, we analyzed the relationship between SP-cluster area and spine head area. Both genotypes showed a strong positive correlation between the two parameters (Figure 8e). Linear regression revealed a non-significant trend for TNF-mutants to have relatively smaller SP-clusters when comparing equally sized spine heads.

4 | DISCUSSION

In the present study, we analyzed the effects of constitutive TNF-deficiency on the structure of dendritic spines. The rationale behind this question were earlier data implicating TNF in the modulation of synaptic transmission and the fine-tuning of excitation/inhibition balance of synaptic networks (Heir & Stellwagen, 2020; Santello & Volterra, 2012; Stellwagen et al., 2005). Although basal levels of TNF are low, complete absence of TNF may impair these physiological functions in synaptic transmission and may cause changes in network activity accompanied by structural alterations. Since some TNF-effects may require SP/spine apparatus (Maggio & Vlachos, 2018), we also investigated SP in spines of TNF-deficient neurons. The main findings of our study can be summarized as follows: (1) Granule cells of TNF-deficient mice have ~20% fewer spines than wildtype controls. (2) TNF-deficient mice have an altered distribution of spine head sizes: they show higher fractions of large and of small spines. (3) Although the fraction of SP+ spines was comparable between genotypes, TNF-deficient mice exhibited larger SP+ spines with larger SP clusters. (4) Small SP− spines were smaller in TNF-deficient mice compared to controls. This pattern of changes suggests that granule cells of TNF-deficient mice have fewer afferent synapses and that the reduced number of synapses is homeostatically compensated for by an increase in head size and SP cluster size of the remaining spines (Figure 9).

4.1 | Structural alterations of spines in TNF-deficient mice are similar to changes observed after entorhinal denervation

This pattern of changes, that is, fewer spines and larger SP+ spines, is very similar to homeostatic changes observed after entorhinal denervation of granule cells. In this experimental denervation model, granule cell spine density is significantly reduced following entorhinal deafferentation (Caceres & Steward, 1983; Vlachos, Becker, et al., 2012; Vuksic et al., 2011) and the loss of spines is homeostatically compensated for by an increase in synaptic strength and an increase in SP-cluster size of the remaining spines (Vlachos, Becker, et al., 2012; Vlachos, Ikenberg, et al., 2013). Such a homeostatic response may help to keep denervated neurons within their physiological firing range (Platschek et al., 2016) and may promote information flow through a partially denervated brain area (Deller & Frotscher, 1997; Steward, 1994).

In the present study focusing on TNF-deficient granule cells we recognized a comparable situation, since the reduced density of spines of TNF-deficient granule dendrites in the outer molecular layer of the dentate gyrus is indicative of a reduced excitatory innervation from the entorhinal cortex. How this reduced innervation comes about and which developmental processes may underlie this change in this constitutive knock-out mouse model is currently unknown and a limitation of our study. Although a developmental role of TNF or even a retraction of some spines into the shaft cannot be fully excluded, we consider it more likely that alterations in the balance of network excitation/inhibition could have caused secondary changes in the density of dendritic spines. This interpretation is in line with studies linking spinogenesis and spine density to afferent activity (Drakew et al., 1996; Engert & Bonhoeffer, 1999; Jourdain et al., 2003; Knott et al., 2006; Maletic-Savatic et al., 1999; Nägerl et al., 2004; Segal et al., 2003). Regardless of the cause, as (i) most spines of adult neurons are innervated (Knott et al., 2006), and, (ii) excitatory input on adult spiny neurons terminates almost exclusively on spines (Mates & Lund, 1983), a reduced density of spines is a bona fide structural indicator of a reduced glutamatergic innervation of granule cells in the dentate gyrus of TNF-deficient mice.

In addition to a reduced spine density, TNF-deficient neurons show an increase in the size of large spines. These spines are characterized by large PSDs (Harris et al., 1992), a high density of AMPA-R (Béïque et al., 2006; Matsuzaki et al., 2001, 2004; Noguchi et al., 2011; Zito et al., 2009), and (this study) by large SP-clusters. Thus, they are strong spines, contributing much to the excitatory drive of a neuron. In contrast, many small spines lack AMPA-R and may represent "silent spines" (Kerchner & Nicoll, 2008). These spines are weak spines, contributing

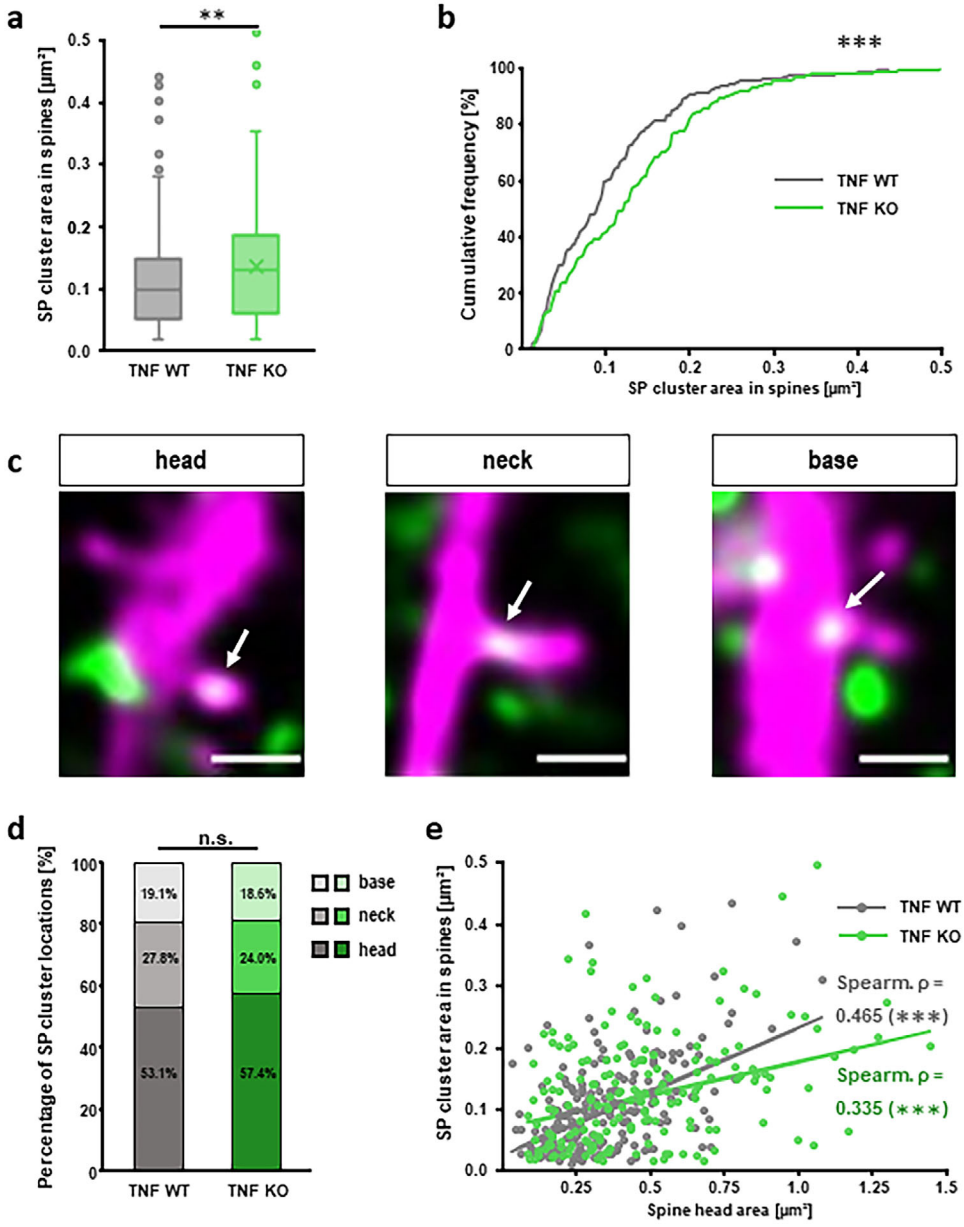

FIGURE 8 SP cluster size is increased in spines of TNF-deficient granule cells. (a) Box plots of Area of SP clusters in SP+ spines. SP clusters were ~33% larger in TNF-KO mice (~0.13 μm^2, $n = 183$) compared to TNF-WT (~0.10 μm^2, $n = 209$) spines. $^{**}p = 0.0018$; Brunner–Munzel *U*-test. (b) Cumulative frequency plot of SP cluster areas for both genotypes. $^{***}p < 0.001$, Cramer–von Mises test. (c) Higher magnifications of dendritic segments of a TNF-WT mouse immunolabeled for SP. SP clusters were found in the head, neck, or base of spines (arrows). Scale bars = 1 μm. (d) Localization of SP clusters in TNF-WT and TNF-KO mice. TNF-WT: 53.1/27.8/19.1%, head/neck/base; TNF-KO: 57.4/24.0/18.6%, head/neck/base. TNF-WT $n = 209$; TNF-KO = 183 clusters; n.s. $p = 0.652$. *G*-test of independence. (e) SP cluster area is positively correlated to spine head area in both genotypes. TNF-WT: 99% confidence interval of Spearman's $\rho = 0.306$ to 0.60; TNF-KO: 99% confidence interval of Spearman's $\rho = 0.153$ to 0.511. Lines represent robust linear regressions of SP cluster area on spine head size. Regression slopes were not significantly different between genotypes, i.e. confidence intervals do overlap: TNF-WT: 0.208, 95% confidence interval = 0.144–0.263 TNF-KO: 0.107, 95% confidence interval = 0.064–0.148

little to the excitatory drive. Since both parameters, that is, spine head size (Matsuzaki et al., 2001; Noguchi et al., 2011; Zito et al., 2009) as well as the presence of SP-clusters (Vlachos et al., 2009), are positively correlated with AMPA-R density, an increase in the spine head area of SP+ spines is a bona fide structural indicator of increased synaptic strength of this spine population. In sum, we see a pattern of changes in the mutants strikingly similar to what we observed under experimental denervation conditions, suggesting that TNF-deficient granule cells compensate a reduction in spine density—indicative of a reduced entorhinal innervation—by homeostatically increasing the size and SP content—indicative of increased synaptic strength—of their remaining spines.

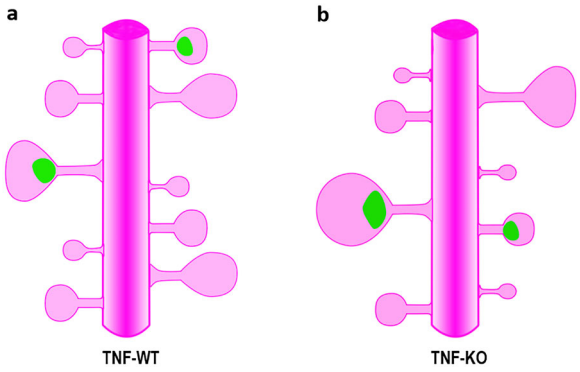

FIGURE 9 Summary diagram illustrating the structural differences between dendritic segments of TNF-WT and TNF-KO granule cells (a, b) TNF-KO dendrites exhibit ~20% fewer spines compared to controls. Although average spine head area is not significantly different, the size distribution of spines has changed: Compared to controls, the fraction of large spines as well as the average size of large spines is increased in the KO. The fraction of small spines is also increased, but this group of spines showed a decreased average head size. Thus, the KO exhibits relatively more large spines, which are also larger and at the same time more small spines, which are also smaller. These bidirectional changes explain why average spine head size between genotypes is not significantly different. Furthermore, large spines were found to be associated with the plasticity-related protein Synaptopodin (green clusters). The larger spines of TNF-KO mice also exhibited larger SP clusters

4.2 | TNF and SP/spine apparatus are linked

TNF and SP have been previously linked in the context of inflammation (Strehl et al., 2014) and Hebbian plasticity (Maggio & Vlachos, 2018). In the first context, that is, inflammation and high levels of TNF, SP was found to be negatively regulated, whereas in the second context, that is, Hebbian plasticity, TNF required SP for its plasticity-promoting effect. This complex relationship may be explained by the divergent effects of TNF at different concentrations: high concentrations of TNF are present in the context of inflammation, whereas lower concentrations of TNF modulate synaptic plasticity under physiological conditions (Heir & Stellwagen, 2020; Santello & Volterra, 2012). Thus, the relationship between TNF and SP may depend on the specific condition of an experiment, that is, whether TNF is present in high concentrations, for example, inflammation, slightly elevated concentrations, for example, plasticity conditions, or constitutively, for example, in naive animals.

In this study, we used a constitutive TNF-deficient mouse and found that TNF-deficiency was associated with larger SP-clusters in spines compared to wildype. A trivial explanation of this result is that TNF and SP are negatively correlated. This interpretation contrasts, however, with earlier observations, in which parallel increases in glial TNF (Becker et al., 2013) and SP-cluster size (Vlachos, Ikenberg, et al., 2013) were reported following entorhinal denervation, suggesting that TNF and SP are positively correlated in this condition. We speculate that the compensatory increase in SP cluster size seen in constitutively TNF-deficient mice may not be the result of TNF-deficiency. Rather, other regulators of homeostatic synaptic plasticity, such as retinoic acid (Lenz et al., 2021), which enlarges both spine heads as well as SP clusters, could contribute to these changes. Further in vitro and in vivo experiments are required to resolve the question, whether the increase in SP cluster sizes seen in the present study is the result of TNF-deficiency or the result of denervation-related adaptations.

4.3 | Competitive interactions between strong and weak spines may underlie the decrease in size of small spines

The increased average size of large spines was accompanied by a reduced average size of small spines. This reduction in size could be the result of competitive interactions between the large and strong SP+ spines and spines in their neighbourhood: Large SP+ spines can compete with newly formed spines via a NMDA-R/CaMKII-dependent mechanism (Vlachos, Helias et al., 2013) and may reduce them in size. This interaction takes the precise temporal correlation of calcium entering the cell into account (Helias et al., 2008). Such a mechanism would be homeostatic in nature, since it keeps the average spine head size constant. Indeed, as was shown recently (Jungenitz et al., 2018), granule cells control spine head size across their dendritic arbour. In this earlier study, high-frequency stimulation of the middle molecular layer of the dentate gyrus caused LTP and an increase in spine head size in the stimulated zone. In the nonstimulated outer molecular layer, however, dendritic segments of the same granule cell exhibited a decrease in spine head size (Jungenitz et al., 2018), indicative of hetereosynaptic long-term depression (LTD) in this layer (Abraham & Bear, 1996; Christie & Abraham, 1992; Jedlicka et al., 2015). Thus, the decrease in the average size of small spines may be secondary to the increase in the strength of large SP+ spines.

4.4 | Changes of spine density and size may contribute to learning and memory deficits of TNF-deficient mice

The behavior of constitutive TNF-deficient mice has been studied and an impaired learning and memory retention performance were reported (Baune et al., 2008). It is conceivable that the structural changes we report here contribute to such behavioral deficits. A reduction of granule cell spine density by ~20% is significant and may be associated with a reduced excitatory drive onto dentate granule cells. Furthermore, the compensatory strengthening of some synapses, while keeping the neuron within a physiologic firing range, could also limit the degrees of freedom a granule cell has for plasticity. Since synaptic information storage capacity has been linked to spine size classes (Bromer et al., 2018), it is conceivable that homostatically enlarged and highly stable SP+ spines are saturated in this respect, that is they cannot be strengthened further and do not contribute to informational changes induced by plasticity. The concomitant reduction of the fraction of medium sized

spines, i.e. of those spines able to undergo both structural LTP as well as structural LTD, may further limit the ability of TNF-deficient granule cells to express plasticity and may thus diminish their ability to integrate into neuronal ensembles encoding novel contexts (Abdou et al., 2018).

ACKNOWLEDGMENTS

We thank Charlotte Nolte-Uhl and Anke Biczysko for technical support and Dr. Meike Fellenz for help with the intracellular injection method. This work was supported by the bilateral Croatian-German project (Ministry of Science and Education of the Republic of Croatia and Deutscher Akademischer Austauschdienst (MZOŠ-DAAD) to M.V. and T.D.), Deutsche Forschungsgemeinschaft (DFG CRC 1080 to T.D.), the Scientific Centre of Excellence for Basic, Clinical and Translation Neuroscience (project "Experimental and clinical research of hypoxic-ischemic damage in perinatal and adult brain"; GA KK01.1.1.01.007 funded by the European Union through the European Regional Development Fund), Europass Mobility grant (to D.S.) and Dr. Senckenbergische Stiftung (to T.D.).

CONFLICT OF INTEREST

TD received funding from Novartis for a lecture on human brain anatomy. The other authors declare that the research was conducted in the absence of any commercial or financial relationships that could be constructed as a potential conflict of interest.

AUTHORS CONTRIBUTIONS

DS, MR, MV acquired data, DS and AD analyzed data, TD and MV conceived and supervised the study, TD, DS, AD, and MV wrote the manuscript with contributions from all authors. All authors were involved in data interpretation and critically revising the manuscript. All authors read and approved the final manuscript.

DATA AVAILABILITY STATEMENT

The data that support the findings of this study are available from the corresponding author upon reasonable request.

PEER REVIEW

The peer review history for this article is available at https://publons.com/publon/10.1002/cne.25237.

ORCID

Thomas Deller https://orcid.org/0000-0002-3931-2947

REFERENCES

Abdou, K., Shehata, M., Choko, K., Nishizono, H., Matsuo, M., Muramatsu, S.-I., & Inokuchi, K. (2018). Synapse-specific representation of the identity of overlapping memory engrams. *Science (New York, N.Y.)*, *360*(6394), 1227–1231. https://doi.org/10.1126/science.aat3810

Abraham, W. C., & Bear, M. F. (1996). Metaplasticity: The plasticity of synaptic plasticity. *Trends in Neurosciences*, *19*(4), 126–130. https://doi.org/10.1016/s0166-2236(96)80018-x

Arends, J. J., & Jacquin, M. F. (1993). Lucifer yellow staining in fixed brain slices: Optimal methods and compatibility with somatotopic markers in neonatal brain. *Journal of Neuroscience Methods*, *50*(3), 321–339. https://doi.org/10.1016/0165-0270(93)90039-t

Bas Orth, C., Vlachos, A., Del Turco, D., Burbach, G. J., Haas, C. A., Mundel, P., Feng, G., Frotscher, M., & Deller, T. (2005). Lamina-specific distribution of Synaptopodin, an actin-associated molecule essential for the spine apparatus, in identified principal cell dendrites of the mouse hippocampus. *The Journal of Comparative Neurology*, *487*(3), 227–239. https://doi.org/10.1002/cne.20539

Baune, B. T., Wiede, F., Braun, A., Golledge, J., Arolt, V., & Koerner, H. (2008). Cognitive dysfunction in mice deficient for TNF- and its receptors. *American Journal of Medical Genetics. Part B, Neuropsychiatric Genetics: The Official Publication of the International Society of Psychiatric Genetics*, *147B*(7), 1056–1064. https://doi.org/10.1002/ajmg.b.30712

Beattie, E. C., Stellwagen, D., Morishita, W., Bresnahan, J. C., Ha, B. K., von Zastrow, M., Beattie, M. S., & Malenka, R. C. (2002). Control of synaptic strength by glial TNFalpha. *Science (New York, N.Y.)*, *295*(5563), 2282–2285. https://doi.org/10.1126/science.1067859

Becker, D., Zahn, N., Deller, T., & Vlachos, A. (2013). Tumor necrosis factor alpha maintains denervation-induced homeostatic synaptic plasticity of mouse dentate granule cells. *Frontiers in Cellular Neuroscience*, *7*, 257. https://doi.org/10.3389/fncel.2013.00257

Béïque, J.-C., Lin, D.-T., Kang, M.-G., Aizawa, H., Takamiya, K., & Huganir, R. L. (2006). Synapse-specific regulation of AMPA receptor function by PSD-95. *Proceedings of the National Academy of Sciences of the United States of America*, *103*(51), 19535–19540. https://doi.org/10.1073/pnas.0608492103

Bonhoeffer, T., & Yuste, R. (2002). Spine Motility. *Neuron*, *35*(6), 1019–1027. https://doi.org/10.1016/S0896-6273(02)00906-6

Bromer, C., Bartol, T. M., Bowden, J. B., Hubbard, D. D., Hanka, D. C., Gonzalez, P. V., Kuwajima, M., Mendenhall, J. M., Parker, P. H., Abraham, W. C., Sejnowski, T. J., & Harris, K. M. (2018). Long-term potentiation expands information content of hippocampal dentate gyrus synapses. *Proceedings of the National Academy of Sciences of the United States of America*, *115*(10), E2410–E2418. https://doi.org/10.1073/pnas.1716189115

Brunner, E., & Munzel, U. (2000). The nonparametric behrens-fisher problem: Asymptotic theory and a small-sample approximation. *Biometrical Journal*, *42*(1), 17–25. https://doi.org/10.1002/(SICI)1521-4036(200001)42:1<17::AID-BIMJ17>3.0.CO;2-U

Caceres, A., & Steward, O. (1983). Dendritic reorganization in the denervated dentate gyrus of the rat following entorhinal cortical lesions: A Golgi and electron microscopic analysis. *The Journal of Comparative Neurology*, *214*(4), 387–403. https://doi.org/10.1002/cne.902140404

Christie, B. R., & Abraham, W. C. (1992). Priming of associative long-term depression in the dentate gyrus by θ frequency synaptic activity. *Neuron*, *9*(1), 79–84. https://doi.org/10.1016/0896-6273(92)90222-y

DeFelipe, j., Conti, F., van Eyck, S. L., & Manzoni, T. (1988). Demonstration of glutamate-positive axon terminals forming asymmetric synapses in cat neocortex. *Brain Research*, *455*(1), 162–165. https://doi.org/10.1016/0006-8993(88)90127-8

Deller, T., Merten, T., Roth, S. U., Mundel, P., & Frotscher, M. (2000). Actin-associated protein synaptopodin in the rat hippocampal formation: Localization in the spine neck and close association with the spine apparatus of principal neurons. *The Journal of Comparative Neurology*, *418*(2), 164–181. https://doi.org/10.1002/(sici)1096-9861(20000306)418:2<164::aid-cne4>3.0.co;2-0

Deller, T., & Frotscher, M. (1997). Lesion-induced plasticity of central neurons: Sprouting of single fibres in the rat hippocampus after unilateral entorhinal cortex lesion. *Progress in Neurobiology*, *53*(6), 687–727. https://doi.org/10.1016/s0301-0082(97)00044-0

Deller, T., Korte, M., Chabanis, S., Drakew, A., Schwegler, H., Stefani, G. G., Zuniga, A., Schwarz, K., Bonhoeffer, T., Zeller, R., Frotscher, M., & Mundel, P. (2003). Synaptopodin-deficient mice lack a spine apparatus and show deficits in synaptic plasticity. *Proceedings of the National Academy of Sciences of the United States of America*, *100*(18), 10494–10499. https://doi.org/10.1073/pnas.1832384100

Drakew, A., Muĺller, M., Gaĺhwiler, B. H., Thompson, S. M., & Frotscher, M. (1996). Spine loss in experimental epilepsy: Quantitative light and electron microscopic analysis of intracellularly stained CA3 pyramidal cells in hippocampal slice cultures. *Neuroscience*, *70*(1), 31–45. https://doi.org/10.1016/0306-4522(95)00379-w

Dunaevsky, A., Blazeski, R., Yuste, R., & Mason, C. (2001). Spine motility with synaptic contact. *Nature Neuroscience*, *4*(7), 685–686. https://doi.org/10.1038/89460

Engert, F., & Bonhoeffer, T. (1999). Dendritic spine changes associated with hippocampal long-term synaptic plasticity. *Nature*, *399*(6731), 66–70. https://doi.org/10.1038/19978

Fifková, E., & van Harreveld, A. (1977). Long-lasting morphological changes in dendritic spines of dentate granular cells following stimulation of the entorhinal area. *Journal of Neurocytology*, *6*(2), 211–230. https://doi.org/10.1007/BF01261506

Friedrich, S., Konietschke, F., & Pauly, M. (2019). Resampling-based analysis of multivariate data and repeated measures designs with the R package MANOVA.RM. *The R Journal*, *11*(2), 380–400. https://doi.org/10.32614/RJ-2019-051

Gray, E. G. (1959). Axo-somatic and axo-dendritic synapses of the cerebral cortex: An electron microscope study. *Journal of Anatomy*, *93*(Pt 4), 420–433.

Grigoryan, G., & Segal, M. (2016). Ryanodine-mediated conversion of STP to LTP is lacking in synaptopodin-deficient mice. *Brain Structure & Function*, *221*(4), 2393–2397. https://doi.org/10.1007/s00429-015-1026-7

Harris, K. M., Jensen, F. E., & Tsao, B. (1992). Three-dimensional structure of dendritic spines and synapses in rat hippocampus (CA1) at postnatal day 15 and adult ages: Implications for the maturation of synaptic physiology and long-term potentiation [published erratum appears in J Neurosci 1992 Aug;12(8):Following table of contents]. *The Journal of Neuroscience*, *12*(7), 2685–2705. https://doi.org/10.1523/JNEUROSCI.12-07-02685.1992

Heir, R., & Stellwagen, D. (2020). Tnf-Mediated homeostatic synaptic plasticity: From in vitro to in vivo models. *Frontiers in Cellular Neuroscience*, *14*, 565841. https://doi.org/10.3389/fncel.2020.565841

Helias, M., Rotter, S., Gewaltig, M.-O., & Diesmann, M. (2008). Structural plasticity controlled by calcium based correlation detection. Helias@bccn.Uni-freiburg.De. *Frontiers in Computational Neuroscience*, *2*, 7. https://doi.org/10.3389/neuro.10.007.2008

Hick, M., Herrmann, U., Weyer, S. W., Mallm, J.-P., Tschäpe, J.-A., Borgers, M., Mercken, M., Roth, F. C., Draguhn, A., Slomianka, L., Wolfer, D. P., Korte, M., & Müller, U. C. (2015). Acute function of secreted amyloid precursor protein fragment APPsα in synaptic plasticity. *Acta Neuropathologica*, *129*(1), 21–37. https://doi.org/10.1007/s00401-014-1368-x

Holtmaat, A., Bonhoeffer, T., Chow, D. K., Chuckowree, J., de Paola, V., Hofer, S. B., Hübener, M., Keck, T., Knott, G., Lee, W.-C. A., Mostany, R., Mrsic-Flogel, T. D., Nedivi, E., Portera-Cailliau, C., Svoboda, K., Trachtenberg, J. T., & Wilbrecht, L. (2009). Long-term, high-resolution imaging in the mouse neocortex through a chronic cranial window. *Nature Protocols*, *4*(8), 1128–1144. https://doi.org/10.1038/nprot.2009.89

Jedlicka, P., Benuskova, L., & Abraham, W. C. (2015). Computational modeling of heterosynaptic plasticity in the hippocampus. *BMC Neuroscience*, *16*(S1). https://doi.org/10.1186/1471-2202-16-S1-P1

Jedlicka, P., & Deller, T. (2017). Understanding the role of synaptopodin and the spine apparatus in Hebbian synaptic plasticity - New perspectives and the need for computational modeling. *Neurobiology of Learning and Memory*, *138*, 21–30. https://doi.org/10.1016/j.nlm.2016.07.023

Jedlicka, P., Schwarzacher, S. W., Winkels, R., Kienzler, F., Frotscher, M., Bramham, C. R., Schultz, C., Orth, C. B., & Deller, T. (2009). Impairment of in vivo theta-burst long-term potentiation and network excitability in the dentate gyrus of synaptopodin-deficient mice lacking the spine apparatus and the cisternal organelle. *Hippocampus*, *19*(2), 130–140. https://doi.org/10.1002/hipo.20489

Jourdain, P., Fukunaga, K., & Muller, D. (2003). Calcium/calmodulin-dependent protein kinase II contributes to activity-dependent filopodia growth and spine formation. *The Journal of Neuroscience*, *23*(33), 10645–10649. https://doi.org/10.1523/JNEUROSCI.23-33-10645.2003

Jungenitz, T., Beining, M., Radic, T., Deller, T., Cuntz, H., Jedlicka, P., & Schwarzacher, S. W. (2018). Structural homo- and heterosynaptic plasticity in mature and adult newborn rat hippocampal granule cells. *Proceedings of the National Academy of Sciences of the United States of America*, *115*(20), E4670-E4679. https://doi.org/10.1073/pnas.1801889115

Kasai, H., Fukuda, M., Watanabe, S., Hayashi-Takagi, A., & Noguchi, J. (2010). Structural dynamics of dendritic spines in memory and cognition. *Trends in Neurosciences*, *33*(3), 121–129. https://doi.org/10.1016/j.tins.2010.01.001

Kasai, H., Matsuzaki, M., Noguchi, J., Yasumatsu, N., & Nakahara, H. (2003). Structure–stability–function relationships of dendritic spines. *Trends in Neurosciences*, *26*(7), 360–368. https://doi.org/10.1016/S0166-2236(03)00162-0

Kerchner, G. A., & Nicoll, R. A. (2008). Silent synapses and the emergence of a postsynaptic mechanism for LTP. *Nature Reviews. Neuroscience*, *9*(11), 813–825. https://doi.org/10.1038/nrn2501

Knott, G. W., Holtmaat, A., Wilbrecht, L., Welker, E., & Svoboda, K. (2006). Spine growth precedes synapse formation in the adult neocortex in vivo. *Nature Neuroscience*, *9*(9), 1117–1124. https://doi.org/10.1038/nn1747

Korkotian, E., Frotscher, M., & Segal, M. (2014). Synaptopodin regulates spine plasticity: Mediation by calcium stores. *The Journal of Neuroscience: The Official Journal of the Society for Neuroscience*, *34*(35), 11641–11651. https://doi.org/10.1523/JNEUROSCI.0381-14.2014

Lenz, M., Kruse, P., Eichler, A., Straehle, J., Beck, J., Deller, T., & Vlachos, A. (2021). All-trans retinoic acid induces synaptic plasticity in human cortical neurons. *eLife*, *10*, e63026.

Locksley, R. M., Killeen, N., & Lenardo, M. J. (2001). The TNF and TNF receptor superfamilies. *Cell*, *104*(4), 487–501. https://doi.org/10.1016/s0092-8674(01)00237-9

Maggio, N., & Vlachos, A. (2018). Tumor necrosis factor (TNF) modulates synaptic plasticity in a concentration-dependent manner through intracellular calcium stores. *Journal of Molecular Medicine (Berlin, Germany)*, *96*(10), 1039–1047. https://doi.org/10.1007/s00109-018-1674-1

Maletic-Savatic, M., Malinow, R., & Svoboda, K. (1999). Rapid dendritic morphogenesis in CA1 hippocampal dendrites induced by synaptic activity. *Science (New York, N.Y.)*, *283*(5409), 1923–1927. https://doi.org/10.1126/science.283.5409.1923

Mates, S. L., & Lund, J. S. (1983). Neuronal composition and development in lamina 4C of monkey striate cortex. *The Journal of Comparative Neurology*, *221*(1), 60–90. https://doi.org/10.1002/cne.902210106

Matsuzaki, M., Ellis-Davies, G. C., Nemoto, T., Miyashita, Y., Iino, M., & Kasai, H. (2001). Dendritic spine geometry is critical for AMPA receptor expression in hippocampal CA1 pyramidal neurons. *Nature Neuroscience*, *4*(11), 1086–1092. https://doi.org/10.1038/nn736

Matsuzaki, M., Honkura, N., Ellis-Davies, G. C. R., & Kasai, H. (2004). Structural basis of long-term potentiation in single dendritic spines. *Nature*, *429*(6993), 761–766. https://doi.org/10.1038/nature02617

McKinney, R. A. (2010). Excitatory amino acid involvement in dendritic spine formation, maintenance and remodelling. *The Journal of Physiology*, *588*(Pt 1), 107–116. https://doi.org/10.1113/jphysiol.2009.178905

Mundel, P., Heid, H. W., Mundel, T. M., Krüger, M., Reiser, J., & Kriz, W. (1997). Synaptopodin: An actin-associated protein in telencephalic dendrites and renal podocytes. *The Journal of Cell Biology*, *139*(1), 193–204. https://doi.org/10.1083/jcb.139.1.193

Nägerl, U. V., Eberhorn, N., Cambridge, S. B., & Bonhoeffer, T. (2004). Bidirectional activity-dependent morphological plasticity in hippocampal neurons. *Neuron*, *44*(5), 759–767. https://doi.org/10.1016/j.neuron.2004.11.016

Noguchi, J., Nagaoka, A., Watanabe, S., Ellis-Davies, G. C. R., Kitamura, K., Kano, M., Matsuzaki, M., & Kasai, H. (2011). In vivo two-photon uncaging

of glutamate revealing the structure-function relationships of dendritic spines in the neocortex of adult mice. *The Journal of Physiology*, *589*(Pt 10), 2447–2457. https://doi.org/10.1113/jphysiol.2011.207100

Paul, M. H., Choi, M., Schlaudraff, J., Deller, T., & Del Turco, D. (2020). Granule cell ensembles in mouse dentate gyrus rapidly upregulate the plasticity-related protein synaptopodin after exploration behavior. *Cerebral Cortex (New York, N.Y. : 1991)*, *30*(4), 2185–2198. https://doi.org/10.1093/cercor/bhz231

Platschek, S., Cuntz, H., Vuksic, M., Deller, T., & Jedlicka, P. (2016). A general homeostatic principle following lesion induced dendritic remodeling. *Acta Neuropathologica Communications*, *4*, 19. https://doi.org/10.1186/s40478-016-0285-8

R Core Team (2013). *R: A language and environment for statistical computing*. R Foundation for Statistical Computing, Vienna, Austria. http://www.R-project.org/

Santello, M., Bezzi, P., & Volterra, A. (2011). Tnfα controls glutamatergic gliotransmission in the hippocampal dentate gyrus. *Neuron*, *69*(5), 988–1001. https://doi.org/10.1016/j.neuron.2011.02.003

Santello, M., & Volterra, A. (2012). Tnfα in synaptic function: Switching gears. *Trends in Neurosciences*, *35*(10), 638–647. https://doi.org/10.1016/j.tins.2012.06.001

Schindelin, J., Arganda-Carreras, I., Frise, E., Kaynig, V., Longair, M., Pietzsch, T., Preibisch, S., Rueden, C., Saalfeld, S., Schmid, B., Tinevez, J.-Y., White, D. J., Hartenstein, V., Eliceiri, K., Tomancak, P., & Cardona, A. (2012). Fiji: An open-source platform for biological-image analysis. *Nature Methods*, *9*(7), 676–682. https://doi.org/10.1038/nmeth.2019

Segal, M., Greenberger, V., & Korkotian, E. (2003). Formation of dendritic spines in cultured striatal neurons depends on excitatory afferent activity. *The European Journal of Neuroscience*, *17*(12), 2573–2585. https://doi.org/10.1046/j.1460-9568.2003.02696.x

Spacek, J. (1985). Three-dimensional analysis of dendritic spines. Ii. Spine apparatus and other cytoplasmic components. *Anatomy and Embryology*, *171*(2), 235–243. https://doi.org/10.1007/bf00341418

Steinmetz, C. C., & Turrigiano, G. G. (2010). Tumor necrosis factor-α signaling maintains the ability of cortical synapses to express synaptic scaling. *The Journal of Neuroscience : The Official Journal of the Society for Neuroscience*, *30*(44), 14685–14690. https://doi.org/10.1523/JNEUROSCI.2210-10.2010

Stellwagen, D., Beattie, E. C., Seo, J. Y., & Malenka, R. C. (2005). Differential regulation of AMPA receptor and GABA receptor trafficking by tumor necrosis factor-alpha. *The Journal of Neuroscience : The Official Journal of the Society for Neuroscience*, *25*(12), 3219–3228. https://doi.org/10.1523/JNEUROSCI.4486-04.2005

Stellwagen, D., & Malenka, R. C. (2006). Synaptic scaling mediated by glial TNF-alpha. *Nature*, *440*(7087), 1054–1059. https://doi.org/10.1038/nature04671

Steward, O. (1994). *"Reorganization of neuronal circuitry following central nervous system trauma: Naturally occurring processes and opportunities for therapeutic intervention": The neurobiology of central nervous system trauma*. Oxford University Press.

Strehl, A., Lenz, M., Itsekson-Hayosh, Z., Becker, D., Chapman, J., Deller, T., Maggio, N., & Vlachos, A. (2014). Systemic inflammation is associated with a reduction in Synaptopodin expression in the mouse hippocampus. *Experimental Neurology*, *261*, 230–235. https://doi.org/10.1016/j.expneurol.2014.04.033

Stück, E. D., Christensen, R. N., Huie, J. R., Tovar, C. A., Miller, B. A., Nout, Y. S., Bresnahan, J. C., Beattie, M. S., & Ferguson, A. R. (2012). Tumor necrosis factor alpha mediates GABA(A) receptor trafficking to the plasma membrane of spinal cord neurons in vivo. *Neural Plasticity*, *2012*, 261345. https://doi.org/10.1155/2012/261345

Vlachos, A., Becker, D., Jedlicka, P., Winkels, R., Roeper, J., & Deller, T. (2012). Entorhinal denervation induces homeostatic synaptic scaling of excitatory postsynapses of dentate granule cells in mouse organotypic slice cultures. *Plos One*, *7*(3), e32883. https://doi.org/10.1371/journal.pone.0032883

Vlachos, A., Helias, M., Becker, D., Diesmann, M., & Deller, T. (2013). Nmda-receptor inhibition increases spine stability of denervated mouse dentate granule cells and accelerates spine density recovery following entorhinal denervation in vitro. *Neurobiology of Disease*, *59*, 267–276. https://doi.org/10.1016/j.nbd.2013.07.018

Vlachos, A., Ikenberg, B., Lenz, M., Becker, D., Reifenberg, K., Bas-Orth, C., & Deller, T. (2013). Synaptopodin regulates denervation-induced homeostatic synaptic plasticity. *Proceedings of the National Academy of Sciences of the United States of America*, *110*(20), 8242–8247. https://doi.org/10.1073/pnas.1213677110

Vlachos, A., Korkotian, E., Schonfeld, E., Copanaki, E., Deller, T., & Segal, M. (2009). Synaptopodin regulates plasticity of dendritic spines in hippocampal neurons. *The Journal of Neuroscience*, *29*(4), 1017–1033. https://doi.org/10.1523/JNEUROSCI.5528-08.2009

Vlachos, A., Müller-Dahlhaus, F., Rosskopp, J., Lenz, M., Ziemann, U., & Deller, T. (2012). Repetitive magnetic stimulation induces functional and structural plasticity of excitatory postsynapses in mouse organotypic hippocampal slice cultures. *The Journal of Neuroscience*, *32*(48), 17514–17523. https://doi.org/10.1523/JNEUROSCI.0409-12.2012

Vuksic, M., Del Turco, D., Vlachos, A., Schuldt, G., Müller, C. M., Schneider, G., & Deller, T. (2011). Unilateral entorhinal denervation leads to long-lasting dendritic alterations of mouse hippocampal granule cells. *Experimental Neurology*, *230*(2), 176–185. https://doi.org/10.1016/j.expneurol.2011.04.011

Yap, K., Drakew, A., Smilovic, D., Rietsche, M., Paul, M. H., Vuksic, M., Del Turco, D., & Deller, T. (2020). The actin-modulating protein synaptopodin mediates long-term survival of dendritic spines. *ELife*, *9*, e62944. https://doi.org/10.7554/eLife.62944

Yuste, R., & Denk, W. (1995). Dendritic spines as basic functional units of neuronal integration. *Nature*, *375*(6533), 682–684. https://doi.org/10.1038/375682a0

Zhang, X., Pöschel, B., Faul, C., Upreti, C., Stanton, P. K., & Mundel, P. (2013). Essential role for synaptopodin in dendritic spine plasticity of the developing hippocampus. *The Journal of Neuroscience : The Official Journal of the Society for Neuroscience*, *33*(30), 12510–12518. https://doi.org/10.1523/JNEUROSCI.2983-12.2013

Zito, K., Scheuss, V., Knott, G., Hill, T., & Svoboda, K. (2009). Rapid functional maturation of nascent dendritic spines. *Neuron*, *61*(2), 247–258. https://doi.org/10.1016/j.neuron.2008.10.054

How to cite this article: Smilovic, D., Rietsche, M., Drakew, A., Vuksic, M., & Deller, T. (2021). Constitutive tumor necrosis factor (TNF)-deficiency causes a reduction in spine density in mouse dentate granule cells accompanied by homeostatic adaptations of spine head size. *Journal of Comparative Neurology*, 1–14. https://doi.org/10.1002/cne.25237